In Vivo Wireless Powering of a Long-Acting Nanofluidic Drug Delivery Implant

In Vivo Wireless Powering of a Long-Acting Nanofluidic Drug Delivery Implant

Fabiana Del Bono, *Member, IEEE*, Nicola Di Trani, Ashley Joubert, Camden Caffey, Andrea Dentis, *Graduate Student Member, IEEE*, Danilo Demarchi, *Senior Member, IEEE*, Alessandro Grattoni, and Paolo Motto Ros, *Member, IEEE*

***Abstract*—Wireless power transfer (WPT) is a key enabler for long-term operation of implantable medical devices, eliminating the need for percutaneous drivelines and frequent surgical device replacements. This paper presents the design and validation of a fully wireless, rechargeable implantable drug delivery system (nDS) with an integrated power management and control system, specifically developed for use in freely moving animal models. The proposed system consists of a subcutaneous implant with an inductive power receiver and an external, backpack-mounted power transmitter that dynamically adjusts energy delivery in response to real-time implant feedback. A closed-loop power control strategy, implemented via Bluetooth Low Energy (BLE) communication, ensures adaptive power transfer to maintain system efficiency despite coil misalignment and animal movement. Building on a previously characterized inductive link, the present work extends the validation from benchtop characterization to in vivo operation in freely moving rats, demonstrating safe and repeatable wireless battery recharging of an implantable nanofluidic drug delivery system. Across four in vivo recharging sessions, the median average power transfer efficiency during constant-current phase was 22.9% with a median average power delivered to the load of 104.7 mW. The charging sessions lasted from 90 (first) to 30 (last) minutes, performed once per week over 4 weeks. The proposed closed-loop WPT implementation enabled reliable battery recharging within clinically relevant time scales while maintaining operation in compliance with thermal safety constraints, thereby supporting chronic, fully untethered drug delivery studies in small animals.**

***Index Terms*—Wireless power transfer, implantable drug delivery, power management, Bluetooth low energy, bioelectronics, in vivo experiments.**

Received 2 October 2025; revised 7 December 2025 and 14 January 2026; accepted 14 January 2026. Date of publication 22 January 2026; date of current version 29 May 2026. This work was supported by Houston Methodist (AG). This paper was recommended by Associate Editor S. J. Kim. *(Corresponding authors: Alessandro Grattoni; Paolo Motto Ros.)*

Fabiana Del Bono, Andrea Dentis, Danilo Demarchi, and Paolo Motto Ros are with the Department of Electronics and Telecommunications, Politecnico di Torino, 10129, Turin, Italy (e-mail: paolo.mottoros@polito.it).

Nicola Di Trani, Ashley Joubert, and Camden Caffey are with the Department of Nanomedicine, Houston Methodist Research Institute, Houston, TX 77030 USA.

Alessandro Grattoni is with the Department of Nanomedicine, Department of Surgery, and Department of Radiation Oncology, Houston Methodist Hospital, Houston, TX 77030 USA (e-mail: agrattoni@houstonmethodist.org).

Color versions of one or more figures in this article are available at http://doi.org/10.1109/TBCAS.2026.3656748.

Digital Object Identifier 10.1109/TBCAS.2026.3656748

I. Introduction

ACTIVE Implantable Medical Devices (AIMDs) are conceived to enable personalized, long-term therapeutic interventions for the treatment and management of chronic conditions, with telemedicine capabilities [1], [2]. Thanks to new, ever evolving capabilities in device miniaturization, energy harvesting techniques, and integration with connected medical systems [3] these technologies are progressively becoming essential in the clinics. A key challenge in AIMD development is achieving energy autonomy. Primary batteries offer limited capacity and require surgical replacement of the implant, which can be clinically unfeasible or undesirable due to procedural risks, costs, and the impracticality of repeated surgeries. These limitations affect the acceptability and widespread use of the technology. Wireless power transfer (WPT) provides a non-invasive alternative to device replacement, enabling periodic power delivery or battery recharging [4]. Among WPT approaches, inductive coupling is the most established for untethered powering of implants due to its technological maturity [5], [6]. However, at power levels exceeding tens of milliwatts, inductive power transfer may increase the risk of tissue heating, on which safety standards set a 2 °C threshold [7]. Only a few FDA-approved implantable devices currently incorporate wireless recharging [8], [9], [10]. In vivo validation is essential to assess safety, performance, and functionality. However, wireless power studies in freely moving animals are often constrained by experimental setups, such as cage-based transmission coils, which limit scalability for chronic studies and large cohorts [11], [12], [13], [14]. These limitations are particularly restrictive for experimental tests with devices requiring continuous operation in long-term studies, where repeated anesthesia or restraint is unfeasible.

This work addresses these challenges by integrating a feedback-controlled WPT system into an experimental implantable drug delivery platform. The system is designed to enable autonomous operation in freely moving animals, supporting chronic in vivo experimentation. The Nanochannel Delivery System (nDS) is an implantable platform engineered for long-acting controlled drug release, enabling tunable therapeutic delivery over extended periods [15], [16]. It consists of a refillable subcutaneous reservoir and a silicon nanofluidic membrane that passively regulates drug diffusion.

In prior studies, the nDS allowed for remote monitoring and voltage-mediated modulation of drug transport via combined steric and electrostatic effects [17], [18], [19], [20], [21]. Unlike mechanically actuated delivery systems, the nDS employs solid-state electrochemical control, offering compactness and energy efficiency suitable for miniaturized AIMDs [22], [23].

To support electronic actuation and communication, a WPT system was implemented to provide safe, reliable recharging under in vivo conditions [24], [25]. Previous work on this module focused on the design of a closed-loop Near-Field Resonant Inductive Coupling (NRIC) [25] only. In that context, we demonstrated a battery charging approach based on commercial-off-the-shelf (COTS) components that can be scaled to next-generation implants with autonomous communication, characterizing system efficiency for different receiving coils under conditions of misalignment and presence of biological tissue. Moreover, we achieved proof-of-concept and thermally safe recharge of a battery under controlled conditions, proving suitability for future implantation. Additionally, a further step toward system-level validation was reported in [26], which investigated preliminary system integration, while still primarily focusing on the characterization of each key component of the implantable device. In particular, we characterized membrane current, battery discharge under simulated use conditions, and antenna performance for remote monitoring, as part of an architecture enabling in vivo testing of the drug delivery system. However, these works were limited to benchtop setups and lacked the demonstration of the system over extended periods and in a real use-case scenario.

This paper presents the development of a fully-packed, subcutaneous rechargeable implant, complemented by a wearable backpack for testing on rodents and a monitoring system for real-time data collection. These elements form a scalable, IoT-based infrastructure for remote implant management and data acquisition. System development is holistically addressed detailing hardware, firmware and software. The remote monitoring and recharge capabilities are demonstrated in a pilot study on freely moving rats. Preliminary safety assessments on the proposed hardware, as well as the in vivo evaluation of behavioural tolerability and tissue response, complement this study towards a clinically translatable device. Finally, the modular and scalable architecture hereby presented supports multi-animal studies and can be adapted for other AIMD designs featuring similar energy and communication capabilities.

The paper is organized as follows: Section II describes the system architecture, including implant design, transmitter configuration, and power management strategy; Section III details system characterization in terms of power consumption and transfer efficiency; Section IV presents pilot in vivo validation in freely moving rats. Section V discusses the results, system limitations, and potential improvements; conclusions and future directions are summarized in Section VI.

II. Methods and Materials

A. System Overview and Requirements

The device must be biocompatible and suitable for preclinical studies in animal models. From a functional standpoint, the device should enable tunable drug delivery and the monitoring of relevant biological parameters. Remote control of the implant is essential to enable large-scale experiments across multiple animals, allowing for individualized monitoring and the customization of drug release profiles. Rodents, specifically rats, are commonly adopted to assess device performances in a preclinical setting, which imposes constraints in terms of size and weight.

The implants should ensure energy autonomy for several years, with energy storage and power transfer systems designed to be safe, reliable, and consistent throughout the operational lifetime. The WPT system should be robust and flexible, ensuring tolerance to misalignments and relative motion between coils, while remaining responsive. This entails accommodating both rapid variations caused by animal movement and slower changes such as those induced by animal growth or tissue thickening. The system should be designed to minimize the need for surgical procedures or other medical interventions on the animal. Several groups have proposed smart-cage WPT platforms, in which large multi-coil transmitters are integrated into dedicated cages to provide a relatively uniform magnetic field and continuously power implants in freely moving rodents [12], [27], [28], [29], [30]. While these systems demonstrate high power-transfer efficiency at distances of centimeters, and good tolerance to animal position and orientation, they have higher circuit complexity and require custom cages and infrastructure, limiting scalability to large cohorts. In contrast, in this work we adopt a compact portable backpack-based transmitter, which preserves workflows in the animal facility and is therefore more compatible with extensive testing across multiple animals and with translation to clinical scenarios, where a patient would carry an external powering unit. The portable transmitter allows for proximity between transmitter and receiver coils, bypassing the need for additional resonators and reducing circuit complexity. Backpack-mounted electronics are a well-established solution for chronic experiments in freely moving rats, where battery-powered recording or stimulation systems are housed on the back while the implanted interface is kept as light and simple as possible [31], [32], [33]. This configuration has been widely adopted across neural, spinal and olfactory interfaces. In our work, we build on this paradigm, using for the first time the backpack unit as a stand-alone mobile wireless power transmitter that, worn on demand, can safely and efficiently recharge a fully subcutaneous drug-delivery implant during free behavior.

From an implementation perspective, using Commercially available Off-The-Shelf (COTS) components enables rapid prototyping and an early focus on system-level development, and is therefore preferred. The proposed system design is illustrated in Fig. 1. The drug delivery implant is a subcutaneous device

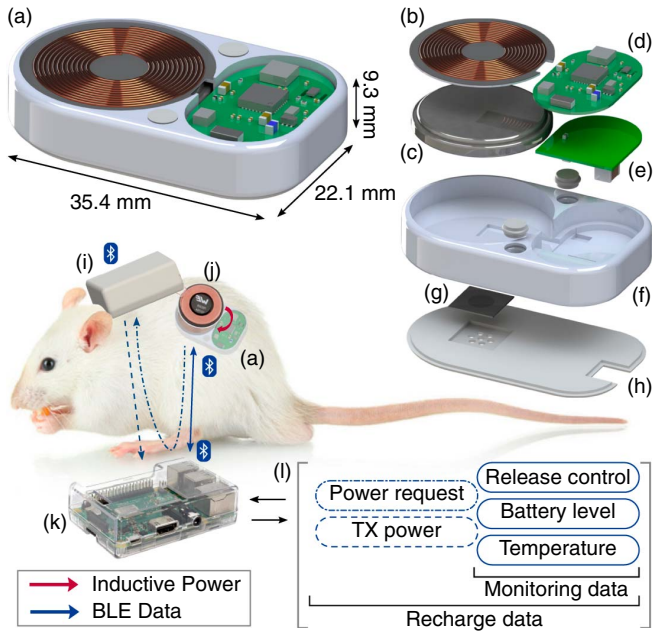

Fig. 1. Overview of the system for chronic experiments: (a-h) nDS Implant, (i-j) External power transmitter, (k-l) External monitoring module. In detail: (a) nDS assembled implant, (b) Power receiver coil, (c) Rechargeable battery, (d) Implant control PCB, (e) Power management PCB, (f) Implant biocompatible case, (g) Silicon nanofluidic membrane for controlled drug delivery, (h) Reservoir lid, (i) Power transmitter wearable backpack, (j) Power transmitter coil for near-field res, (k) Raspberry Pi, (l) Online live-data dashboard. Communication via Bluetooth Low Energy (BLE), (k) in central role, (a) and (i) in peripheral role. Data flow includes bidirectional exchange between (k) and (a), unidirectional data from (a) to (i) through (k) forwarding, and unidirectional data from (i) to (k). Data can be accessed from a remote device connected to the internet through (l).

that integrates the drug release actuator, the drug reservoir, and the electronic circuits required for device operation and drug administration control. The implant is powered by a rechargeable battery and includes a coil for inductive power transfer. Communication is established via Bluetooth Low Energy (BLE). The external infrastructure consists of an IoT-based monitoring system built around a Raspberry Pi and a wearable BLE device used for implant recharging. This IoT architecture enables the configuration of drug release profiles, monitoring of battery status, and temperature sensing during normal operation. When the implant requires wireless battery recharging, the system ensures a thermally safe and energy-efficient process [25]. This is achieved by periodically forwarding power requests from the implant to the wearable transmitter, which in turn provides feedback on the recharging process, allowing remote tracking of charging parameters.

1 Implant description: The subcutaneous nanofluidic drug delivery system (nDS) is shown in Fig. 1(a). It integrates a refillable reservoir, a silicon membrane, and the electronic circuits for control and power management. The voltage-controlled silicon nanofluidic membrane [19] (Fig. 1(g)) is the actuation element for drug release and requires only a few volts for modulation, representing a highly compact actuation solution. It is embedded within the reservoir and electrically connected to the electronic control system (Fig. 1(d)) via internal wiring. The electronic control system regulates the membrane voltage, but also handles temperature sensing and wireless communication. Temperature is monitored as a simple yet meaningful physiological parameter and is critical for assessing compliance with safety standards. A Power Management System (PMS, Fig. 1(e)), is dedicated to power-related functionalities such as battery voltage regulation, wireless charging, and battery monitoring. It also includes a wireless power receiver and a voltage regulator for inductive energy harvesting. The implant is battery-powered (Fig. 1(c)) and equipped with a coil for wireless charging (Fig. 1(b)), enabling fully untethered, long-term operation. The implant is designed with rounded edges and high component packing density. In previous implementations of the nDS platform, the refillable reservoir, the drug-delivery mechanism, and a remote-controlled implant for precise dosing have already been extensively described and validated [19], [34], [35]. In the present work, we therefore only summarize these aspects and focus instead on the system-level integration of the newly introduced inductive wireless power transfer and closed-loop battery-charging architecture, which were not present in earlier nDS versions and represent the main technical advancement.

2 Wireless Power Transmitter description: The power transmitter is designed to dynamically regulate the transmitted power based on real-time feedback from the implant. This ensures stable and safe energy delivery, adapting to the implant's charging needs and minimizing thermal impact. Key design requirements for the charging system include simplicity, compactness, and minimal interference with the animal's natural behavior. The transmitter is housed within a custom-designed backpack worn by the animal. For rodent models, such as rats, this necessitates a lightweight and wireless solution, powered by a battery and constrained in both size and energy capacity. During charging, both the transmitter and the implant operate as Bluetooth Low Energy (BLE) peripherals connected to a central Raspberry Pi. The Raspberry Pi forwards power requests from the implant to the transmitter and logs charging data. These data are then streamed to a PC for real-time visualization and post hoc analysis.

3 IoT monitoring system description: The IoT system is completed by a Raspberry Pi, designed to remain continuously operational within the laboratory infrastructure. Its primary function is to perform continuous animal monitoring through BLE data acquisition and transmission via the MQTT protocol. A dedicated dashboard has been implemented in NodeRed [36] to monitor, control, and acquire data from the whole system through a simple GUI. When required, a dedicated charging algorithm is activated to manage wireless recharge.

B. Hardware

1 Implant:

a) nDS PCB: The nDS printed circuit board (PCB) is responsible for implant control and is designed to operate with an input voltage of $3.0\,\mathrm{V}$. It consists of a two-layer stackup with a total thickness of $0.5\,\mathrm{mm}$. The board has an oval shape with dimensions of $12\,\mathrm{mm} \times 20\,\mathrm{mm}$. It integrates a Texas

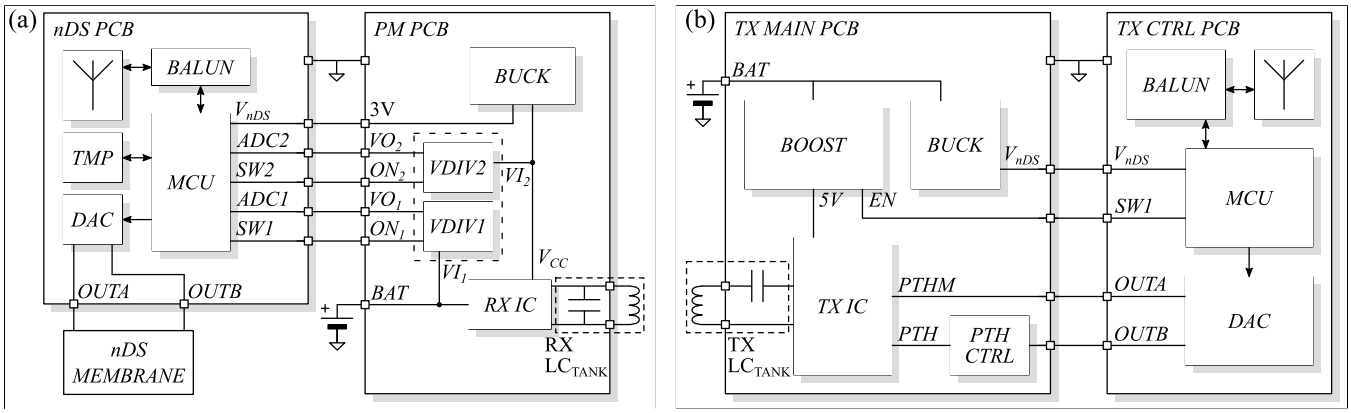

Fig. 2. Block diagram of the electronic system: (a) Implant electronic system, composed of: nDS PCB and RX PCB; (b) Transmitter electronic system, composed of TX Main PCB and TX Control PCB.

Instruments CC2640R2F MCU [37], along with a balun transformer and antenna for BLE communication. The control of the nanofluidic membrane is managed via a dual-output DAC (Maxim Integrated, MAX5532 [38]), and temperature sensing is provided by a dedicated digital sensor (Texas Instruments, TMP117 [39]) (Fig. 2(a)).

The external DAC enables fine control over the membrane's operating states, offering calibration capabilities and customizable drug release profiles. The DAC is dual-output with a maximum output voltage of 3 V. From a power perspective, the MAX5532 features a typical operating current below 5 μA, and can be reduced to approximately 0.5 μA in shutdown mode. Each output is connected to a membrane electrode, allowing the system to select the active channel, invert the polarization, and trigger drug release. The system is capable of sustaining drug release even while the microcontroller remains in standby mode. Similarly, the TMP117 sensor consumes approximately 135 μA during active conversion but supports low-power operation, with typical currents of 1.25 μA in standby and 250 nA in shutdown, making it suitable for continuous low-power monitoring. The temperature sensor is configured to operate in one-shot mode, triggered by the microcontroller as needed and spending the rest of the time in shutdown mode.

b) Power Management Module: The implant's Power Management (PM) module is responsible for handling power delivery, regulating the voltage supplied to the nDS PCB, and managing the battery charging process. The system integrates a wireless power transfer receiver (WPT-RX) based on the LTC4124 integrated circuit (Analog Devices), hereafter referred to as the RX IC, and a Buck DC/DC Converter (Texas Instruments, TPS82740B [40]). These components are specifically designed for compact, low-power applications. The RX IC supports wireless charging in constant-current/constant-voltage (CC-CV) mode [41]. During discharge, it consumes only 7 μA, while shipping mode ensures that the assembled device can preserve battery life indefinitely prior to implantation. The PM module is complemented by a 19 mm diameter coil. The RX IC has been hardware-configured to deliver a charging current of 25 mA at 4.2 V. This configuration was selected as a favorable trade-off among battery safety limits, charging efficiency, and duration. The TPS82740 buck converter is set to provide a nominal 3.0 V output from the 2.7 V to 4.2 V battery: for $V_{\text{IN}} > 3.0$ V it regulates as a buck converter, while as V_{IN} approaches V_{OUT} it enters 100% duty-cycle mode, connecting V_{OUT} to V_{IN} so that, below the 100%-mode threshold, the output tracks the battery voltage instead of remaining regulated.

2 Transmitter: The inductive power transfer implemented is based on a 2-coil Near-Field Resonant Inductive Coupling (NRIC), featuring a compact 20.8 mm diameter coil. The power transmission architecture consists of two, battery powered, main modules: the power delivery module (TX MAIN) and the control module (TX CTRL), as shown in Fig. 2(b).

a) Main Transmitter Module: The TX MAIN module handles power transmission. It includes the Wireless Power Transmitter IC (Analog Devices, LTC4125 [42]), referred to as the TX IC, the power transmission control circuit (PTH CTRL), a boost converter to regulate the input voltage to 5 V for the TX IC, and a buck converter to supply 3 V to the TX CTRL module. The power transfer system based on the LTC4125 IC was chosen for flexibility in matching the resonance of the LC tank. Transmitted power is regulated via voltages applied to the PTHM and PTH1 pins, the latter referred to as PTH. A dedicated, custom, power control circuit [25] is connected to this pin. The TX IC is powered on upon request from the control module by enabling the boost converter through its enable pin. The TX MAIN module is fabricated on a four-layer PCB with a thickness of 1.55 mm and dimensions of 26 mm $\times$ 18 mm. To provide visual feedback during experiments, an LED is included to light up when power transmission is active and correctly functioning.

b) Transmitter Control: The control module is based on a BLE-enabled microcontroller, which manages the activation of the boost converter on the TX MAIN module, controls a dual-output DAC for setting the PTH and PTHM voltages,

and handles communication with the IoT infrastructure. For modularity and convenience, the same PCB used in the implant was reused for this module.

C. Detail on WPT and Power Management

a) Inductive Link Details: The WPT hardware is based on a resonant inductive link operating at 200 kHz, with LC tanks in Series-to-Parallel (SP) configuration [25]. Although it is less efficient, a two-coil structure was chosen over three- or four-coil configurations to prioritize circuit simplicity and avoid complex equipment. On the implant side, the absence of a secondary resonator reduces implant bulk or the need for additional surgeries. The loss in Power Transfer Efficiency (PTE) expected from this choice is compensated by keeping the coil in close proximity by design. Both the TX (Wurth Electronik, 760308101104 [43]) and RX (Würth Elektronik, 760308101214 [44]) coils are commercially available, and their properties are summarized in Table I. Receiver and transmitter coil geometry were selected based on the parametric optimization reported in our previous work on the same NRIC link [25]. In that study, four commercial RX coils with diameters from 6 to 19 mm were characterized in combination with the same TX coil, chosen for size convenience. The 17 mm and 19 mm RX coils exhibited the highest Q-factor while operating well below their self-resonant frequency and, as a result, achieved the best power-transfer efficiency and robustness to misalignment: at a TX–RX distance of 6.5 mm, representative of the expected skin thickness plus packaging, they reached average charging efficiencies above 26% without thermal shutdown thanks to adaptive power delivery, when charging a Li-Ion battery with 10 mA current [25]. Both coils also showed resilience to axial and angular misalignments, maintaining efficiencies above 20% and 25% for misalignments in the ranges 0 mm to 6 mm and 0° to 8°, respectively, and never dropping below 15% up to 6 mm and 8°. In the present work, we therefore select the 19 mm RX coil, which provides the best overall performance maximizing mutual coupling, power-transfer efficiency, and tolerance to misalignment, while remaining within the 20 mm diameter dictated by the battery footprint. The selected coil specifications are summarized in Table I. The resonant frequency is tuned to 200 kHz, using a parallel between two capacitors in series to the coil on the TX side ($C_{TX1} = 68$ nF, $C_{TX2} = 22$ nF) and a single capacitor in parallel to the coil on the RX side ($C_{RX} = 22$ nF). Any shift in resonant frequency introduced by the tissue loading is compensated by the AutoResonant feature of the TX IC, which continuously adjusts its switching frequency to the instantaneous resonant frequency of the LC network, within its 50–250 kHz operating range. As a consequence, any shift in resonant frequency introduced by tissue loading or coil misalignment is automatically tracked by the transmitter, limiting losses in power transfer efficiency.

b) Adaptive Power Transfer: The power management system implements an adaptive control strategy that enables wireless recharging under varying conditions. It works by dynamically regulating the power transmitted based on real-time feedback from the implanted receiver device.

TABLE I
SPECIFICATIONS OF THE INDUCTIVE LINK COIL. THE RESONANT LINK ADOPTS AN SP TOPOLOGY TUNED AT 200 KHZ

Parameter	TX coil	RX coil
Diameter [mm]	20.8	19.0
Inductance L @ 125 kHz [µH]	6.8	26
Q-factor (datasheet) @ 125 kHz	42	25
Q-factor (measured) @ 200 kHz	57.1	30.6
Self-resonant frequency f_{res} [MHz]	20	11

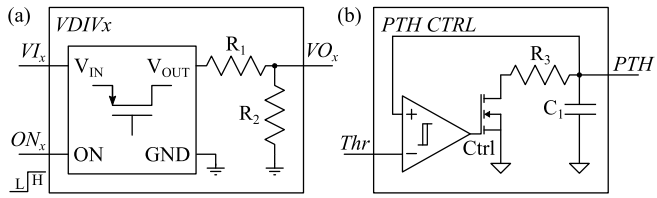

Fig. 3. Electrical schemes of the power management control: (a) Implant voltage monitoring circuit based on voltage dividers; (b) Transmitter power control circuit. $R_1 = 39$ kΩ, $R_2 = 57$ kΩ, $R_3 = 10$ kΩ, $C_1 = 1$ µF.

This approach maximizes power transfer efficiency while minimizing thermal stress, delivering only the necessary power according to the implant's instantaneous demand. The control algorithm relies on two voltages measured at the implant side: V_{CC}, the rectified coil voltage, and V_{BAT}, the battery voltage. No additional components are included for direct current monitoring during charging, in order to minimize both space and power consumption.

c) Implant Voltage Monitoring Circuit: Voltage readings are acquired using the ADC in the implant's MCU. Two voltage divider circuits - referred to as `VDIV` - are used to bring V_{CC} and V_{BAT} within the ADC dynamic range. Dedicated switches, driven by the MCU GPIOs, ensure current flows through the divider only during voltage measurement (Fig. 3(a)).

d) Transmitter Power Control Circuit: Half-bridge mode was selected to drive the TX LC Tank for this low-power application, reducing losses and enabling fine control over the transmitted power. The duration of the switching pulses is proportional to the voltage applied to the `PTH1` pin, while the voltage applied to the `PTHM` pin improves power-up efficiency by setting the minimum pulse width during the power-seeking phase. Control of these voltages is handled via the TX Control DAC. PTH control circuit (PTH CTRL), shown in Fig. 3(b), consists of a comparator, capacitor, and MOSFET, and maintains the `PTH` voltage around the threshold (*Thr*) set by the DAC [25]. The DAC's second output is directly connected to the `PTHM` pin.

e) Preliminary assessment of the WPT link safety: Before finalizing the implementation of a 25 mA charging current, a preliminary thermal validation was performed during a controlled recharge, monitoring the TX coil, RX coil and RX IC temperature. Indeed, compared to previous works where the charging current was set to 10 mA, this current allows for a faster recharge on a higher capacity battery, but increases the risk of overheating the device. The results of this preliminary

TABLE II
PRELIMINARY ANALYSIS OF NRIC LINK HEATING (DISTANCE OF 10 MM)

Charging current (mA)	Medium	$\Delta T_{\text{Tx coil}}$ (°C)	$\Delta T_{\text{Rx coil}}$ (°C)	$\Delta T_{\text{Rx IC}}$ (°C)
10	Air	2.7	0.8	1.1
25	Air	8.2	3.7	4.2
10	Animal tissue	2.6	0.0	0.6
25	Animal tissue	0.2	0.5	2.6

TABLE III
THRESHOLD HANDLING FOR VBAT AND VCC

Measurement	Lower threshold	Upper threshold
V_{BAT}	3.6 V	None
V_{CC}	$V_{\text{BAT}} + 0.2\,\text{V}$	$V_{\text{BAT}} + 0.25\,\text{V}$

TABLE IV
BLE PERIPHERAL SERVICE CHARACTERISTICS

Device	Characteristic	Mode	Size (bytes)
Implant	Membrane voltage	R/W	2
	Implant temperature	R/N	2
	V_{BAT} Voltage	R	2
	V_{CC} Voltage	R	2
	Activate recharge	R/W	1
	Recharge feedback	R/N	1
Transmitter	Command on PTH	R/W	1
	Command	N	1
	PTHM Value	R	2
	Activate recharge	R/W	1

R = Read, W = Write, N = Notify

investigation, presented in Table II, indicate a moderate and acceptable increase with respect to ambient temperature. In parallel, we carried out a preliminary specific absorption rate (SAR) assessment of the inductive link by means of HFSS, using a three-layer tissue model (skin–fat–muscle). The peak spatial-average SAR, evaluated over 1 g of tissue according to the IEEE C95.1 standard [45], was confirmed to be below the $1.6\,\text{W}\,\text{kg}^{-1}$ safety limit. Taken together, HFSS-based SAR simulations and benchtop thermal measurements provided a preliminary confirmation of compliance with RF-exposure and thermal safety constraints prior to in vivo validation and design finalization.

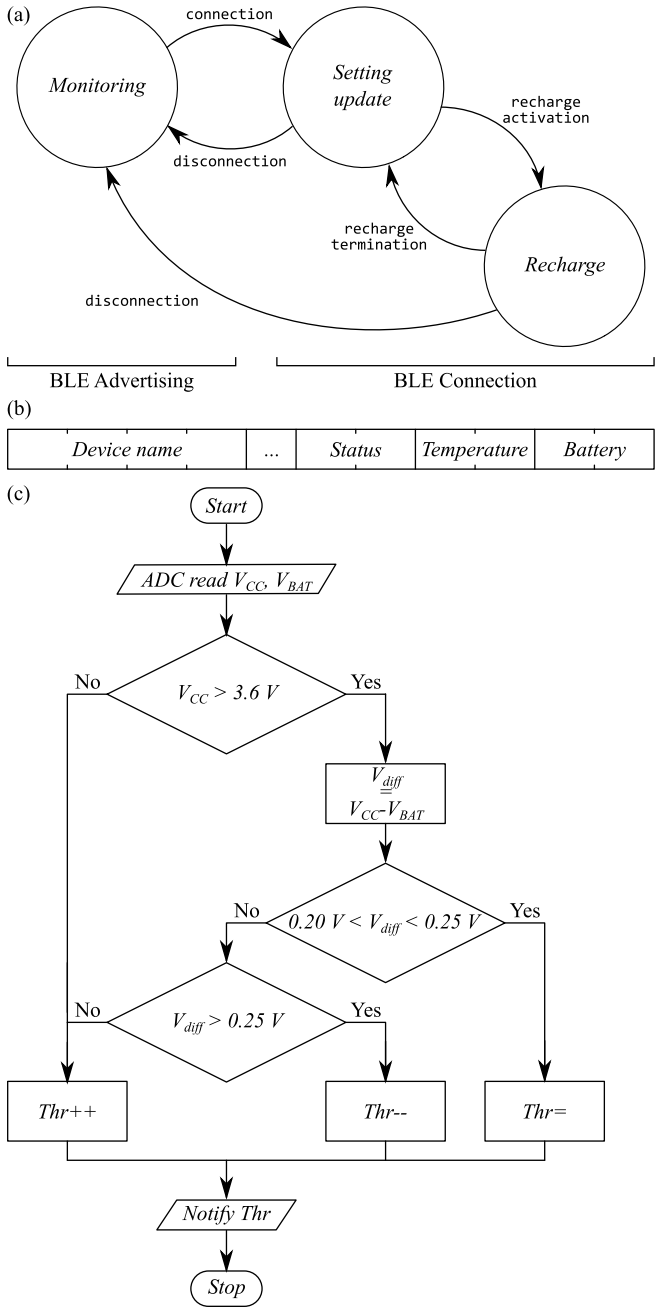

Fig. 4. Implant firmware: (a) High-level state diagram, (b) Scan response data structure, (c) Block diagram of the WPT feedback algorithm.

D. Firmware

The firmware of both the implant and transmitter is based on a Texas Instruments BLE application [46], running on the proprietary operating system TI-RTOS. Both devices operate as BLE peripherals and can be controlled by a BLE device acting in central role. Through BLE services, it is possible to remotely control the functions of each peripheral (Table IV).

1 Implant Firmware: The implant firmware is designed to enable remote monitoring and control, ensure battery longevity, and optimize the charging process.

Timing of individual functions and data availability are managed to minimize energy-intensive operations.

In the context of this work, the Bluetooth firmware logic is described as a state machine, where each state corresponds to a specific function or operational mode of the application. Although the underlying RTOS does not strictly implement this model, the state-machine representation is useful for illustrating the global functional behavior of the system. This abstraction is depicted in Fig. 4(a). The firmware is structured around three main states: *Monitoring*, *Setting Update*, and *Recharge*. The first state overlaps with the BLE advertising (ADV) mode, while

TABLE V
IMPLANT PERIODIC EVENTS PERIODS (MONITORING AND RECHARGE)

Temporized Event	Monitoring	Recharge
Implant temperature	10 min	10 s
V_{BAT} Voltage meas.	10 min	2 s
V_{CC} Voltage meas.	-	2 s
Recharge feedback	-	2 s

the other two are associated with an active BLE connection (CON).

a) Monitoring State: During the *Monitoring* state, the device operates in advertising mode, periodically broadcasting data packets to signal its presence and provide basic status information. This mode is sufficient for remote monitoring, as it allows data acquisition without requiring user interaction or high system responsiveness. The BLE advertising packets include basic information for device identification (e.g., device name), and upon scan request, additional data are provided via scan response packets, including device name, drug release status, implant temperature, and battery voltage (Fig. 4(b)). The advertising interval is set to 2 s in order to minimize antenna activation and transmission time, while guaranteeing an acceptable discoverability. Between two advertising events, the system enters a low-power sleep mode, waking only for scheduled tasks. Periodic events in this mode include temperature and battery voltage measurements, both performed every 10 min (Table V).

b) Setting Update State: When a BLE connection is established, the device allows access to its configuration through a dedicated BLE service, summarized in Table IV. One characteristic encodes the membrane voltage as a 2-byte value, specifying the DAC output and the active channel (i.e., polarization) [26]. Additional read-only characteristics report the measured values of implant temperature, battery voltage (V_{BAT}), and the rectified coil voltage (V_{CC}).

c) Recharge State: Wireless power transfer can be activated from the connected state by writing to a specific characteristic. Entering the *Recharge* state alters the periodic measurement schedule: temperature and battery voltage readings become more frequent, V_{CC} is continuously monitored, and notifications are enabled to transmit feedback to the power transmitter. The timing parameters for this mode are detailed in Table V. A disconnection event or a write command to a designated characteristic triggers charge termination and restores the low-power timing.

d) Recharge algorithm: The charging feedback algorithm is illustrated in the diagram in Fig. 4(c). The algorithm runs periodically every 2 s. At each iteration, the implant measures $\mathrm{V_{CC}}$, which must reach at least 3.6 V. If this condition is not met, the implant requests an increase in transmitted power by adjusting the TX threshold value THR. If $\mathrm{V_{CC}}$ exceeds 3.6 V, the algorithm evaluates the voltage difference $V_{\mathrm{diff}} = V_{\mathrm{CC}} - V_{\mathrm{BAT}}$. For efficient and reliable charging, V_{diff} should fall within the range 200 mV to 250 mV [25]. If the difference lies within this range, the TX threshold THR is maintained. If it falls outside, the system increases or decreases THR accordingly, depending on whether V_{diff} is below or above the target range.

2 Transmitter Firmware: The transmitter also operates as a BLE peripheral, enabling optimal remote control through a centralized device. The transmitter BLE service is summarized in Table IV.

The transmitter remains continuously active in advertising mode. During idle periods, the boost converter - and consequently the power transmission module it supplies - is turned off to reduce power consumption.

Upon establishing a BLE connection, charging can be initiated and terminated by writing to a designated characteristic, which triggers an enable signal to the boost converter. At this point, the DAC is activated and initialized with a default value of 150 mV. The transmitter then enters a listening state, awaiting commands to update the power threshold (THR) characteristic, forwarded by the Raspberry Pi in response to feedback notifications from the implant. The THR value is incremented in discrete steps of 3 mV, up to a maximum of 1 V, which is defined as the safety limit. The microcontroller updates the DAC outputs to set the new values for PTH and PTHM. Once updated, the transmitter makes PTHM available and notifies the set value through the command characteristic (Table IV). When charging is terminated, all DAC outputs are reset to their default values.

E. Software

The device management software is coded in Python and runs on a Raspberry Pi. All devices present in the laboratory facility are monitored through an IoT system built on a Python-based software architecture. The main application logic module performs continuous scanning of advertising packets, filters recognized devices based on a preconfigured MAC address list, decodes the content of scan response packets, and processes structured data such as temperature, battery level, and drug release status. In addition to data acquisition, the system can also receive remote commands and forward them to the appropriate BLE devices after initiating a connection. In parallel, MQTT communication manages subscription to command topics and periodically publishes the collected BLE data in a structured format, enabling access by other clients. The entire system is configurable through JSON files that define network and system parameters, supported BLE devices, and recognized command sets.

The charging module manages communication control between the nDS (implant) and TX (transmitter) devices via BLE connection. Upon user request, the program establishes a connection and configures the peripherals' characteristics to initiate the charging process. Specifically, it enables notifications and activates recharge mode on the implant, and initiates power transmission from the TX. During the operational cycle, the software receives threshold (THR) notifications from the nDS and forwards the command to the TX. It then reads the parameters set on both the implant and the TX, logging all data. The acquired parameters include

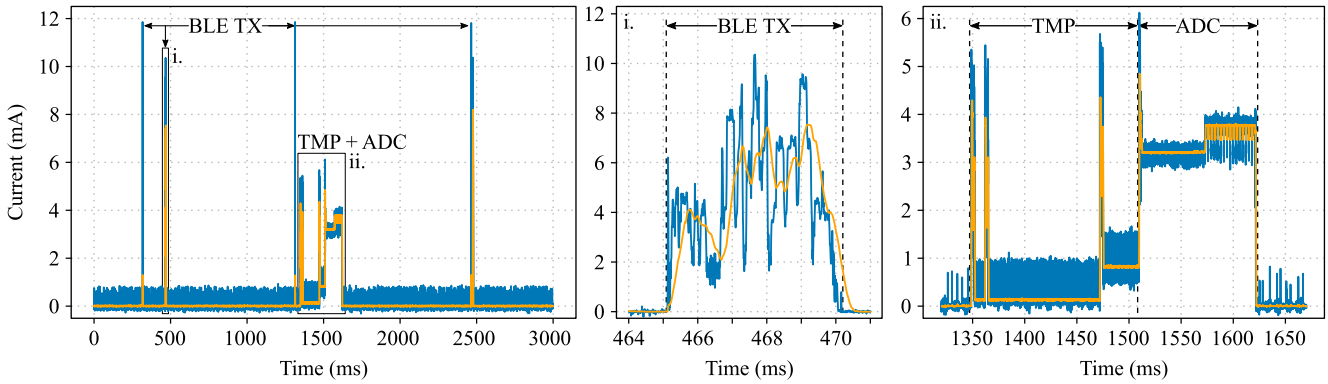

Fig. 5. nDS PCB current absorption waveforms and corresponding MCU events during normal operation in monitoring mode. Blue line is the measured current. Yellow line is the denoised signal filtered with moving average.

battery and supply voltages, internal device temperature, and estimated transmitted power, which are stored for subsequent analysis. For optimal charge control, the software additionally calculates a real-time estimate of the instantaneous transmitted power P_{TX}, calculated using a regression curve obtained during wireless power transfer characterization [25]. The relationship between the PTH value and transmitted power is modeled as approximately linear, as $P_{TX} = m \cdot \mathrm{PTH} + q$ with $m = 1.19$ and $q = 12.81$. This approach enables indirect monitoring of the charging current and supports appropriate decisions on charge termination. When the user requests charge termination, the system disables notifications and disconnects both devices.

III. System Performance Results

A. Implant

1) Power consumption analysis: The system was characterized to verify energy optimization strategies and estimate battery lifetime. Current and voltage measurements were sampled using a Keithley DMM7510 digital multimeter [47], with the system powered by a battery charged to 3.6 V.

A current consumption test was performed on the nDS PCB operating in BLE advertising mode, with event timing configured to capture all characteristic activities. The resulting profile is shown in Fig. 5. Characteristic events are identifiable: for BLE antenna transmission (BLE TX), temperature sensor readings (TMP), and ADC sampling. As expected, three transmission events occur every 2 s, corresponding to advertising over the three BLE channels. Using a moving average filter and a signal segmentation algorithm, characteristic events were isolated and their power contribution calculated, relative to the baseline (Table VI). This allowed estimation of total power consumption under different use scenarios.

For the operating timing parameters (Table V), the total average current drawn by the device in BLE advertising mode was 18.7 μA, distributed as follows: 32.1% baseline current, 63.8% BLE TX events, 3.4% ADC events, and 0.6% TMP events. Repeating the same analysis to capture baseline and TX events during a BLE connection, the average current increased to 95.4 μA, with the following distribution: 3.7% baseline current, 95.5% BLE TX events, 0.7% ADC events and 0.1% TMP events.

TABLE VI
Average Current and Power Consumption per Event

Event	Avg. Current (mA)	Avg. Power (mW)
Baseline	0.006	0.018
TX	3.650	10.9
ADC	3.420	10.3
TMP	0.437	1.31

With the same methodology, measurements were repeated including the Power Management PCB. Estimates were calculated for both ADV and CON modes, inspecting the temporizations for monitoring and charging use cases. Power consumption was estimated considering the regulated 3.0 V at the nDS input and at 3.6 V from the battery the RX board input. The results are reported in Fig. 6, showing absolute power consumption values and conversion efficiency of the RX board. A reference efficiency, obtained on advertising data prior to the optimization of temporizations [26], is also shown for comparison.

a) Power consumption contributions and battery life estimation: Assuming a usage scenario in which the device remains in advertising mode throughout the day, except for a 1-minute connection window to update parameters, the total daily charge consumption on nDS PCB only would amount to 450.1 μA h. The operational lifetime of the system powered by a 40 mA h battery can be estimated: considering a supply voltage of 3.6 V at the RX board and the use of a switching regulator to convert to 3.0 V with the minimum conversion efficiency of 54%, the average charge drawn from the battery goes up to 694.4 μA h. This results in an estimated autonomy of about 57 days.

B. Transmitter

Following a similar strategy as above, transmitter efficiency was evaluated during the actual charging of a battery.

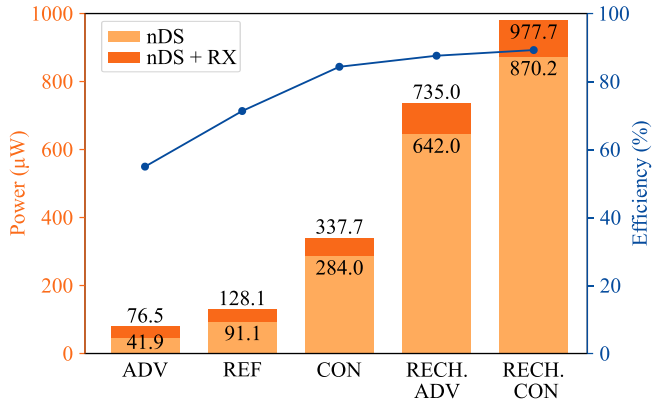

Fig. 6. Implant power consumption analysis under different scenarios: Advertising mode (ADV), Connection mode (CON), Recharge in Advertising (RECH. ADV), Recharge in Connection (RECH. CON), Reference condition (REF, [26]). Power consumption is reported for nDS PCB alone and both nDS and RX PCBs connected in cascade. The efficiency of the RX PCB is calculated as the ratio between the latter and former.

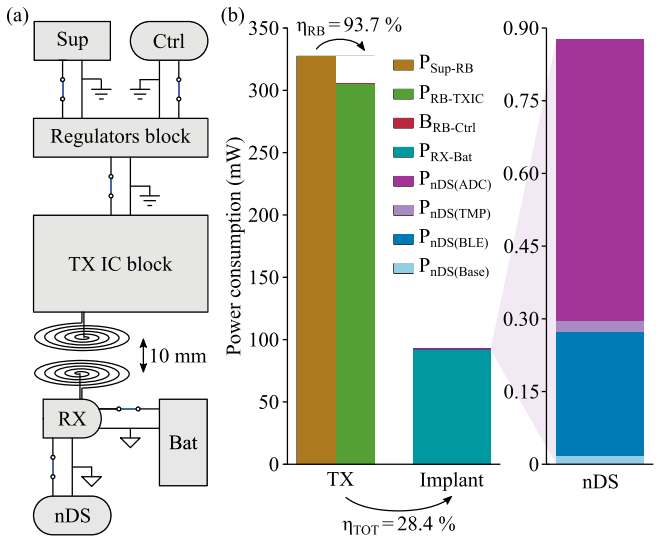

Fig. 7. Power consumption breakdown and efficiency of the WPT system during recharge in controlled conditions. (a) Measurement reference scheme (b) Measurement results, explicitly reporting the regulators block efficiency η_{RB} and the total system efficiency η_{TOT}.

To isolate contributions, a preliminary version of the transmitter was used, consisting of two stacked PCBs - TX IC block and Regulators Block (RB) - along with the control PCB (Fig. 7(a)). The coils were positioned at a fixed distance of 10 mm. The receiver block - identical to that used in previous tests - included the RX board, the nDS device, and a battery. For these tests, a high-capacity battery was used to ensure a stable voltage with minimal drift during the charging period. Current was measured using a Keithley DMM7510 digital multimeter [48], while voltage was monitored with an oscilloscope throughout the charging process, remaining within expected limits. Fig. 7(b) shows the results, obtained multiplying the average input current to each subsystem with the constant supply voltage values: 3.6 V from the battery to the Regulators Block, 3.0 V to the Control PCB and 5.0 V to the Transmitter module (TXIC).

The measured power consumption values were: 0.89 mW for the nDS, 91.79 mW for the battery, 0.79 mW for the control circuit, 305.06 mW for the TXIC, 326.48 mW delivered by the power supply.

These values yield a total system efficiency from supply to implant of 28.39%, calculated as $\eta_{tot} = P_{Implant}/P_{SUP}$, with $P_{Implant} = P_{nDS} + P_{RX}$. The efficiency of the regulator block (η_{RB}) was calculated as $\eta_{RB} = (P_{TXIC} + P_{Ctrl})/P_{SUP}$, resulting in an efficiency of 93.68%. Based on the average power drawn from the power supply - 326.48 mW - and an operating voltage ranging between 3.6 V and 4.2 V, the charge required for each operational cycle lasting 1.6 h can be calculated as $Q = P/V \cdot t$. Substituting the extreme values of the voltage range yields a charge consumption between 124.3 mA h and 145.1 mA h per charging cycle. These estimates provide a key reference for TX battery selection, which should ensure a predefined number of full implant charging cycles but also consider a safety margin, to account for increased power demand under non-ideal conditions, such as coil misalignment.

A lithium-polymer battery (Jauch LP102530JU [49]), with a capacity of 680 mA h, dimensions of 33 mm × 25.5 mm × 10 mm, and weighing approximately 20 g was selected to balance form factor, sufficient capacity for the planned number of charging cycles, and scalability for longer-duration experimental protocols.

IV. In Vivo Recharge Pilot Study

A. Implant and Transmitter Assembly and Setup

1 Design requirements and conceptualization: The wireless power transfer system for in vivo experiments must meet stringent requirements in terms of size, weight, and tolerability by the animal [50].

The system has been specifically designed for experiments involving freely moving rats, with the aim of avoiding sedation and/or anesthesia procedures during the recharging phase. This implies that the system must withstand the animals' natural movement - often vigorous - and be compact and lightweight enough to be carried without causing discomfort.

a) TX Backpack concept: The miniaturized transmitter was designed to fit within a wearable backpack suitable for use on a rat. This approach has been previously proposed in the literature at a conceptual level for wireless power transfer applications [51], and for external or partially implantable instrumentation in the context of drug delivery [52]. However, no fully implemented solutions have been found in the literature that adopt this approach with validated in vivo animal testing.

b) Anatomical considerations: The use of a backpack offers the advantage of ensuring close proximity between small coils through appropriate mechanical design, thereby enabling system miniaturization while maintaining a favorable form factor and ensuring efficient power transfer. The backpack rests on the thoracic cage, allowing the animal full freedom of movement while providing sufficient support and balance without

discomfort. This approach is well established in preclinical research, commonly used for securing transdermal ports and catheter/tether access points.

To accommodate this, a hybrid solution was adopted: the backpack carries the system's weight on the animal's back, while a flexible, outward-extending floating coil reaches and aligns with the implant located in the abdomen.

c) Coil alignment system: To ensure proper alignment and adhesion between the transmitting coil and the implant, a magnetic coupling mechanism was implemented. This approach minimizes the need for straps or other fastening mechanisms around the rat's abdomen - an area that is sensitive, flexible, and highly mobile. Prior to finalizing the design, a practical study was conducted to evaluate the influence of the magnetic components on the wireless charging process and to ensure that no degradation in performance would occur as a result. The selected magnets are neodymium cubes with a side length of $3\,\mathrm{mm}$. The selected magnets are neodymium cubes with a side length of $3\,\mathrm{mm}$. In particular, we conducted a preliminary test to quantify the impact of the magnets on power delivery by performing measurements with and without the magnets, monitoring the power delivered to the load over a charging-voltage range of $2.8\,\mathrm{V}$ to $4.2\,\mathrm{V}$ in $0.1\,\mathrm{V}$ steps and for charging currents of 10 and 25 mA. The observed differences remained within $2.2\% \pm 1.2\%$ in absolute terms on the delivered power.

d) Animal Study and Welfare considerations: The animals involved in this pilot were two healthy male Sprague-Dawley rats, 2 months old at the start of the experiment, with an average weight of approximately $300\,\mathrm{g}$. One was used as test, the other as a control for histological analysis only. No formal sample size calculation was performed due to the exploratory nature of the study. Animals were not randomized to groups. Despite the docile and resilient nature of this strain, the experiment presents behavioral challenges related to animal management. For this reason, the experimental design included the development of a dedicated charging environment, referred to as enrichment cage, aimed at supporting the animal's comfort and cooperation, playing a fundamental role in the success of the experiment [53]. It compensates for potential discomfort by providing environmental stimulation, including animal-safe toys and food rewards, aiming to make the experience more enjoyable and promote animal compliance. All procedures were approved by the Institutional Animal Care and Use Committee (IACUC), approval no. AUP IS00007358, and carried out in compliance with the Animal Welfare Act, PHS Animal Welfare Policy, and the principles of the NIH Guide for the Care and Use of Laboratory Animals. Animals were housed 2 per cage under a 12h light/dark cycle, with ad libitum access to food and water.

2 Implant:

a) Description and design: The implant used for the in vivo charging proof-of-concept includes all components shown in Fig. 1, except for the drug release elements - namely, the reservoir, membrane, lid, and refill ports - which were omitted to simplify the assembly process. The space typically occupied by these components was filled with resin.

Magnets were placed on either side of the coil to assist with alignment.

b) Fabrication and Assembly procedure: The implant casing was fabricated using Low Force Stereolithography (LFS) on a Formlabs Form 3B+ 3D printer, using BioMed Clear resin compatible with certified medical applications [54], [55]. The PCBs were interconnected using ultra-thin wires, minimizing wire length and avoiding unnecessary overlap (Fig. 8(a)). The receiving coil and battery connections were soldered directly to the receiver PCB. All solder joints and exposed metal areas were covered with a biocompatible UV epoxy resin (Epoxy Technologies Inc., OG116 [56]), cured using a UV gun. Following this, the electronic components were stacked, inserted into the 3D-printed case and secured in place with UV-cured resin. The entire implant was then hermetically sealed using biocompatible thermal epoxy (Epotek, MED-302-3M), centrifuged at $1800\,\mathrm{rpm}$ for 3 minutes to remove air bubbles, and subsequently cured at $70\,^{\circ}\mathrm{C}$ for 3 hours to achieve a stable and durable seal. The final assembled devices have overall measured dimensions of $9.3\,\mathrm{mm} \times 22.1\,\mathrm{mm} \times 35.4\,\mathrm{mm}$ and a total weight of $5.3\,\mathrm{g}$ (Fig. 8(b) and (c)).

3 Transmitter: The transmitter is integrated into a wearable backpack, consisting of a jacket [57] and a 3D-printed enclosure, stabilized on the jacket with velcro tape and fastened with elastic bands. The enclosure houses the battery and printed circuit boards, while the transmission coil extends through a side opening (Fig. 8(d–f)). The total weight of the backpack is approximately $30\,\mathrm{g}$, which corresponds to 10% of the rodent weight. This value falls within reportedly well-tolerated range for adult rats, even in the worse-case of continuously worn payloads [33].

4 Experiment design: The experimental timeline was organized with Day 0 defined as the day of implantation. On Day -1, the devices were fully charged, sterilized via immersion in ethanol, and sealed in Phosphate-Buffered Saline (PBS) solution.

On Day 0, the rats were implanted with the devices via a cervical incision followed by the creation of a subcutaneous pocket (Fig. 8(g)). A stabilization period of observation and post-operative care followed.

On Day 14, the surgical clips were removed and, from that point on, the rats were gradually acclimated to the presence of the backpack and instrumentation, pairing device usage with access to the enrichment cage (Fig. 8(h)).

The first charging session was conducted on Day 27. Subsequent charging events took place on Days 34, 41, and 48.

On Day 58, as per protocol, the animals were euthanized and the devices were explanted together with the surrounding fibrotic capsule for subsequent histological and tissue analysis. Tissues were fixed in 10% neutral-buffered formalin and embedded in paraffin. Five ($5\,\mu\mathrm{m}$) slices were cut and stained with Hematoxylin & Eosin (H&E).

B. In Vivo Results

The primary outcome of the study was the feasibility of repeated wireless recharging in vivo. Secondary outcomes

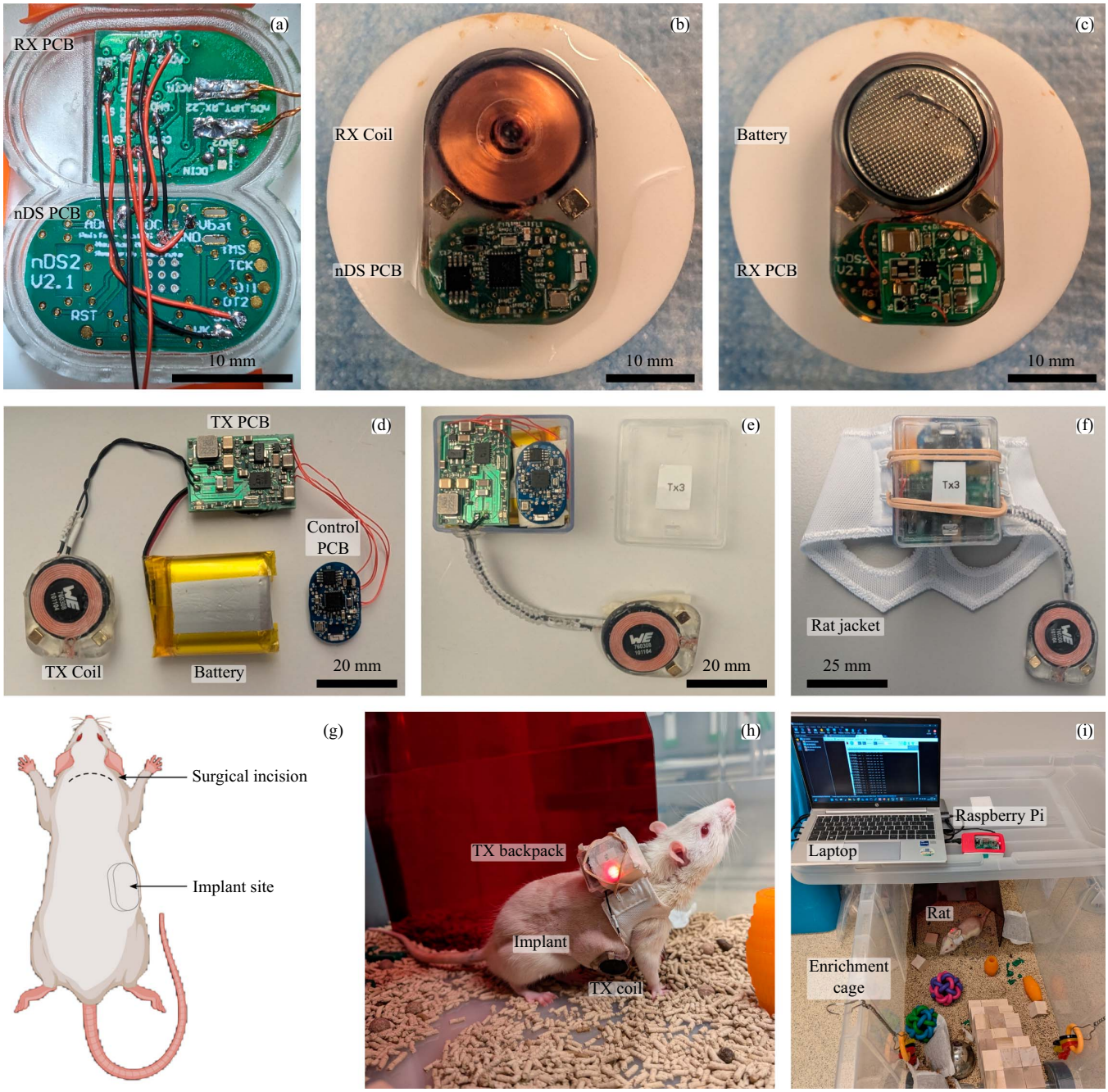

Fig. 8. Experimental setup for in vivo experiments: (a)s Assembly of the implant PCBs (RX and nDS PCB); (b) Assembled implant (top view) showing the coil and nDS PCB; (c) Assembled implant (bottom view) showing the battery and PMS PCB; (d) Assembly of the transmitter components, showing the TX coil, battery, control PCB and TX PCB; (e) Assembly of the transmitter enclosure for the backpack; (f) Final assembly of the backpack including the enclosure with components mounted on the rat jacket; (g) Schematic of the surgical procedure for implantation, highlighting the incision site and implant location; (h) Rat during charging, wearing the backpack with the TX coil aligned to the implant; (i) Experimental setup for in vivo recharge, including Raspberry Pi, laptop, and the rat with the backpack inside the enrichment cage.

included implant thermal performance, tissue response, and behavioral tolerance.

1 Implant monitoring: The results of the in vivo pilot are reported in Fig. 9. Fig. 9(a) shows the battery voltage during discharge, monitored via BLE advertising data. The discontinuities (i-iv) correspond to the scheduled charging sessions. The monitoring system RSSI values ranged from $-45\,\mathrm{dBm}$ to $-91\,\mathrm{dBm}$ (M: $-63.90\,\mathrm{dBm}$, SD: $4.98\,\mathrm{dBm}$). Implant temperature was consistently monitored.

2 Implant Recharge: Fig. 9(b) and (c) shows voltage, estimated TX power and temperature during the first and the remaining three charging sessions, respectively. The dashed lines in the temperature plots indicate the $2\,^{\circ}\mathrm{C}$ range above the baseline temperature.

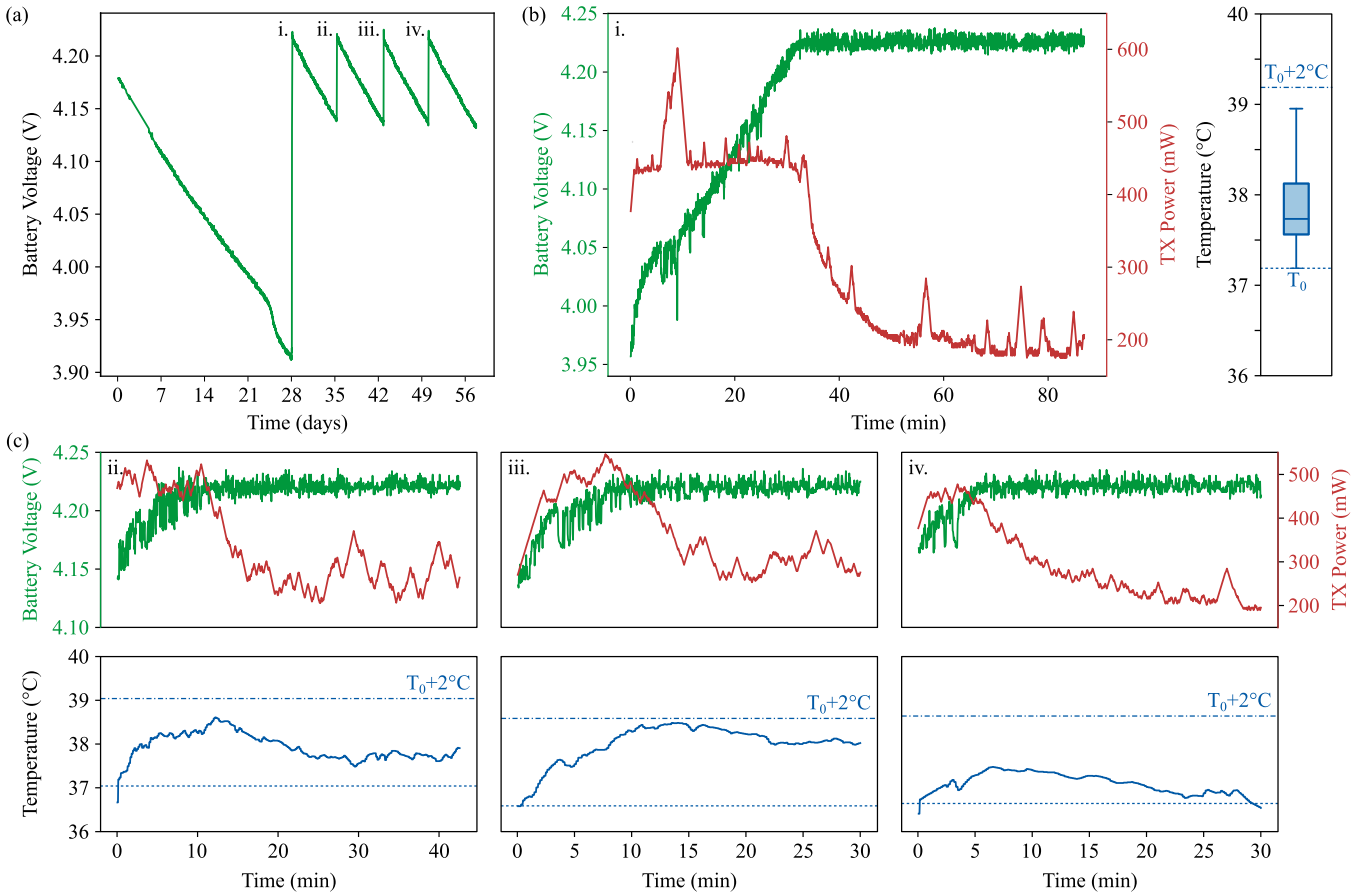

Fig. 9. Proof of concept of in vivo recharge. (a) Discharge data obtained from IoT monitoring system through Scan response data, events (i-iv) correspond to recharge events, detailed in (b-c); (b) Battery voltage, estimated power during the first recharge (i) and temperature; (c) Battery voltage, estimated power and temperature monitoring during second (ii), third (iii) and fourth (iv) recharge.

a) Power Transfer process: During the charging sessions, a clear increase in battery voltage is observed, consistent with the expected charging profile, with minor deviations attributable to measurement noise. This trend is particularly evident during the first charging session.

Transmitted power was estimated in real time from the values read at the PTHM pin, which provide an indirect yet continuous indication of both the implant's power demand and the coupling condition between transmitter and receiver. Variations in this coupling directly affect system efficiency and result in the observed fluctuations in power estimation.

As visible in the first charging session, transmitted power is proportional to the product of voltage and expected current, according to constant-current/constant-voltage (CC-CV) charging profile [25]. The observed decrease in estimated power after the 30-minute mark closely follows the current decay trend recorded during preliminary system characterization [25]. Thus, the power estimate proves to be a reliable qualitative predictor of the charging state, without the need for direct current measurement. To quantify in vivo link performance, the instantaneous overall efficiency $\eta_{\mathrm{TOT}}(t)$ was evaluated during the constant-current phase as the ratio between the power delivered to the load, $P_{\mathrm{DL}}(t) = V_{\mathrm{BAT}}(t)\, I_{\mathrm{CC}}$, and the transmitted power, considering only the initial CC intervals of the four sessions, where the charging current is known and fixed at 25 mA. For each charging session, average values and associated statistics were first computed over the CC interval; median values across sessions are reported here. Across sessions, the median average PTE was 22.9%, with a median standard deviation of 1.4% and median minimum and maximum values of 19.4% and 26.9%, respectively. Over the same intervals, the median average power delivered to the load was 104.7 mW, with median minimum and maximum values of 103.4 mW and 105.6 mW, and a median standard deviation of about 0.5 mW. In detail, the average PTE obtained (mean $\pm$ SD) was $22.4 \pm 1.7\,\%$, $21.8 \pm 1.0\,\%$, $23.8 \pm 4.3\,\%$, and $23.5 \pm 1.1\,\%$ for sessions 1 to 4, respectively. The corresponding power delivered to the load was 101.6 ± 3.9 mW, 104.9 ± 0.5 mW, 104.7 ± 0.6 mW, and 104.8 ± 0.4 mW.

b) System resilience: The power plots allowed to observe instances of misalignment between the transmitting and receiving coils, as the transmitter attempted to compensate for reduced coupling efficiency. The progressive smoothing between sessions may be explained by the effect of the fibrotic capsule, that formed around the implant over time. The progressive thickening of this tissue could have reduced the effectiveness

of the magnetic attraction between the two coils, leading to less abrupt but more persistent displacement.

c) Thermal performance: The recorded temperature closely followed the trend of the transmitted power. The slower rise and decay of temperature compared to the transmitted power can be explained by the thermal capacitance of the implant, as the packaging layers interposed between the IC and the sensor delay heat propagation. In fact, the temperature sensing point within the device is located near its surface, in proximity to the integrated circuit, which has been identified as the primary heat source both in previous studies [24], [25] and in the preliminary bench evaluation summarized in Table II. As such, this location is significant for assessing the thermal exposure of surrounding tissues. Temperature never exceeded a rise of $2\,^{\circ}\mathrm{C}$, the regulatory threshold for this class of devices and a key criterion for in vivo compliance. The improved thermal behavior observed in vivo, compared with the preliminary bench tests in animal tissue, supports the hypothesis that blood perfusion contributes to dissipating heat and mitigating temperature rise in living tissue, as previously discussed in [25].

d) Histological analysis: For preclinical safety assessment of the implant and recharge process, biocompatibility was evaluated. Throughout the duration of the 58-day study, the implants were well tolerated with no observed adverse skin reactions, infection or variation in animal social behavior and mobility. In particular, visual inspection revealed no evidence of skin damage, either from contact with the transmitter or from the pressure exerted by the magnets. Upon explantation, fibrous encapsulation of the implant was observed, indicative of foreign body reaction conventional to medical implants. Overall, there were no signs of significant active inflammatory reaction, suggesting biocompatibility and tolerability. Fibrous capsule thickness remained in the sub-millimeter range, with thick regions of $204 \pm 32\,\mu\mathrm{m}$ and $178 \pm 50\,\mu\mathrm{m}$, and thin regions of $62 \pm 12\,\mu\mathrm{m}$ and $74 \pm 16\,\mu\mathrm{m}$ for the test and control rat, respectively. No evident differences in capsule thickness could be attributed to the wireless recharging procedure.

V. Discussion

Analysis of power consumption and optimization of timing parameters allowed the system to balance energy efficiency with monitoring requirements and device longevity. For temperature and voltage measurements, a 10-minute acquisition interval provided sufficient resolution to detect early signs of local hyperthermia due to local inflammatory responses or late-stage battery discharge while keeping peripheral energy consumption negligible. The use of advertising data combined with selective connection modes effectively extended battery life without compromising monitoring capabilities. The energy use associated with establishing connections during charging was minimal and did not affect the power transfer process, while enabling more stable data exchange and improved responsiveness.

Similarly, the higher data sampling rate during charging, required for safe thermal and electrical monitoring, had only a minor impact on overall energy use. Wireless recharging was successfully demonstrated in vivo in a freely moving rat model. The animal exhibited normal activity and interaction with its environment throughout the study, with no observed behavioral changes or signs of discomfort. Charging reliability was maintained across multiple sessions despite short-term variations in coil alignment due to natural movement and mid-term tissue changes. Fluctuations in transmitted power, efficiency, and temperature across sessions are likely attributable to tissue remodeling around the implant, yet energy delivery remained stable. These results indicate the system's ability to adapt to dynamic in vivo conditions and support its suitability for long-term, freely moving animal studies.

The integration of BLE communication within the closed-loop WPT system enabled real-time monitoring of temperature, battery status, and power transmission efficiency during in vivo operation. This approach eliminated reliance on benchtop instrumentation at the preclinical stage and allowed remote data logging and analysis within an IoT-based infrastructure. Software-based power estimation, used in place of current sensing, provided adequate feedback for safe operation, simplified hardware design, and maintained system performance.

This work demonstrates the feasibility of consistent WPT in freely moving animals, extending previous approaches that were limited to static or tightly controlled environments [11], [12], [13], [14]. The use of a wearable transmitter in a backpack configuration facilitated untethered recharging while preserving animal mobility and welfare, offering a practical solution for chronic studies. Table VII contextualizes our system within the state-of-the-art of WPT platforms for freely moving rodents [12], [27], [28], [29], [30]. Smart-cage solutions, typically operating at $13.56\,\mathrm{MHz}$, achieve higher maximum PTE (up to $\sim 60\%$) at TX–RX distances of several centimeters, but rely on multi-coil arrays, resonant relay structures, and tracking hardware, with system complexity ranging up to more than 20 coils and the need for dedicated cages. In contrast, our backpack-based architecture operates with a single TX–RX pair and no intermediate resonators. By keeping the TX–RX distance limited, it still delivers up to $104.7\,\mathrm{mW}$ at efficiencies between 19.4% and 26.9% (median over sessions). This places its performance within the range of reported systems in terms of delivered power, while substantially reducing circuit and infrastructural complexity. The use of a portable transmitter preserves standard workflows in the animal facility, can be scaled to multi-animal studies by deploying multiple identical backpack units, and better mirrors clinically relevant scenarios, in which a patient would carry an external powering unit, thereby supporting translational potential.

Nonetheless, we acknowledge that our study was limited by the small cohort size, the short observation period, and the lack of integration with drug release functionalities and automation. These results should therefore be interpreted as a pilot proof of feasibility, and more extensive, statistically powered and longitudinal studies on larger cohorts will be required in future work to rigorously validate performance, safety, and inter-animal variability. However, remotely tunable drug delivery using nDS was previously demonstrated by this

TABLE VII
COMPARISON OF INDUCTIVE WPT SYSTEMS FOR FREELY MOVING SMALL ANIMALS

Ref.	Freq. (MHz)	System complexity				$D_{TX\text{-}RX}$ (cm)	PDL (mW)	Max Eff. (%)	Min Eff. (%)
		# Primary TX coils	# Primary Res. coils	# Secondary Res. coils	Tracking system				
[27]	13.56	1	4	1	Kinect	7	24	36.3	16.1
[28]	13.56	1	9	1	–	4	100	59	-
[29]	13.56	1	–	–	Servo with magnetic field sensors	3	1.7	17	1
[12]	13.56	2	2	1	–	7.5	–	14.7	11.5
[30]	13.56	23	–	–	Magnetic tracer for coil activation	7.8	20	31.6	19.6
Our work	0.2	1	–	–	–	0.6	104.7*	26.9*	19.4*

*Median values, calculated across the CC phases of the 4 recharge sessions presented in this work.

group in previous studies [19], [21], [34]. Further investigation is needed to assess the chronic effects of repeated WPT on surrounding biological tissue, including the formation and progression of fibrotic encapsulation and its impact on coupling efficiency and thermal dissipation which in this pilot study did not appear to affect transmission given the negligible capsule thickness observed over the study period. Long-term, multi-subject studies will be necessary to confirm system safety and performance over extended periods. Future work should also focus on further implant miniaturization, such as consolidating power management and control electronics onto a single PCB, which would reduce device footprint, improve manufacturability, and enhance robustness. Although this implementation was tailored to the nanochannel Delivery System (nDS), the design rationale and control strategies are applicable to other experimental Active Implantable Medical Devices (AIMDs) with comparable energy and communication requirements.

VI. CONCLUSION AND FUTURE OUTLOOK

This study demonstrated a wireless power transfer (WPT) system for an implantable drug delivery device, achieving safe and reliable in vivo recharging in freely moving animal models. The integration of a rechargeable implant, wearable transmitter, and IoT-based monitoring infrastructure enabled remote and autonomous operation, maintaining stable performance under dynamic in vivo conditions. The system proved resilient to coil misalignment and subject movement, addressing key challenges in wireless powering of untethered implants and supporting its suitability for long-term preclinical studies. The preliminary safety assessment including SAR analysis, combined with thermal assessment of the implanted system, support the feasibility of scaling this approach towards chronic studies and future clinical translation. The proposed architecture provides a modular framework incorporating energy management strategies and wireless communication that can be adapted to other AIMDs with similar requirements. By eliminating percutaneous drivelines and enabling rechargeable operation, this approach addresses critical constraints in the design of implantable systems, reducing the frequency of surgical interventions and improving the feasibility of chronic studies. Future work should focus on extended multi-subject, long-term studies to assess the chronic effects of repeated WPT on tissue response, including fibrotic encapsulation and its impact on coupling efficiency and thermal dynamics. Additional efforts toward further miniaturization - such as integration of power management and control electronics onto a single PCB - would reduce the device footprint and improve manufacturability. Overall, this work establishes a framework for safe and scalable wireless powering of implantable systems, providing a foundation for advancing AIMDs from preclinical models toward future clinical translation.

ACKNOWLEDGMENT

Thank you to Ilaria Facchi and Gabrielle Rome for their support on animal monitoring and care at HMRI Houston. Thank you to Christian Conti and Luigi Giuffrida for software support. Funding support from HMRI (AG). AG is a co-founder and Chief Scientific Advisor of Continuity Biosciences.

REFERENCES

[1] M. M. Paci et al., "Smart closed-loop drug delivery systems," *Nature Rev. Bioeng.*, vol. 3, pp. 806–834, Oct. 2025, doi: 10.1038/s44222-025-00328-z.
[2] C. Y. X. Chua et al., "Advanced material technologies for space and terrestrial medicine," *Nature Rev. Mater.*, vol. 9, no. 11, pp. 808–821, 2024.
[3] Z. Gao et al., "Advanced energy harvesters and energy storage for powering wearable and implantable medical devices," *Adv. Mater.*, vol. 36, 2024, 1052 Art. no. e2404492. Avilable: https://doi.org/10.1002/adma.202404492
[4] A. B. Amar, A. Kouki, and H. Cao, "Power approaches for implantable medical devices," *Sensors*, vol. 15, pp. 28889–28914, Nov. 2015. Available: https://doi.org/10.3390/s151128889
[5] B. Nelson, S. Karipott, Y. Wang, and K. G. Ong, "Wireless technologies for implantable devices," *Sensors*, vol. 202020, no. 16, Art. no. 4604. Available: https://doi.org/10.3390/s20164604
[6] X. Huang et al., "Materials strategies and device architectures of emerging power supply devices for implantable bioelectronics," *Small*, 2020, Art. no. e1902827.
[7] ""En 45502-1 Active Implantable Medical Devices – Part 1: General Requirements for Safety, Marking and Information to be Provided by the Manufacturer," 1997.
[8] Abbott, "Liberta RC™ DBS System — Redefining Rechargeable," 2025. Accessed: Sep. 2025. [Online]. Available: https://www.neuromodulation.abbott/us/en/healthcare-professionals/movement-disorders/rechargeable-dbs.html
[9] Nevro Corp "Product: Omnia - International English," 2025. Accessed: Sep. 2025. [Online]. Available: https://www.nevro.com/en/providers/product-omnia/
[10] Envoy Medical, "The Esteem® fully implanted active middle ear implant," 2025. Accessed: Sep. 2025. [Online]. Available: https://www.envoymedical.com/esteem

[11] P. McMenamin, U.-M. Jow, M. Kiani, J. R. Manns, and M. Ghovanloo, "A smart cage for behavioral experiments on small freely behaving animal subjects," in *Proc. 6th Int. IEEE/EMBS Conf. Neural Eng. (NER)*, 2013, pp. 985–988.

[12] K. Eom, J. Jeong, T. H. Lee, S. J. Kim, and Y. T. Kim, "A wireless power transmission system for implantable devices in freely moving rodents," *Medical & Biol. Eng. Comput.*, vol. 52, pp. 639–651, Aug. 2014. Available: https://doi.org/10.1007/11517-014-1169-3

[13] R. Sheybani and E. Meng, "On-demand wireless infusion rate control in an implantable micropump for patient-tailored treatment of chronic conditions," in *Proc. 36th Annu. Int. Conf. IEEE Eng. Med. Biol. Soc.*, 2014, pp. 882–885.

[14] A. Cobo, R. Sheybani, H. Tu, and E. Meng, "A wireless implantable micropump for chronic drug infusion against cancer," *Sens. Actuators, A*, vol. 239, pp. 18–25, Mar. 2016.

[15] P. Davoodi et al., "Drug delivery systems for programmed and on-demand release," *Adv. Drug Del. Rev.*, vol. 132, pp. 104–138, Jul. 2018. Available: https://doi.org/10.1016/j.addr.2018.07.002

[16] G. He et al., "Recent progress in implantable drug delivery systems," *Adv. Mater.*, vol. 36, no. 23, 2024, Art. no. e2312530. Available: https://doi.org/10.1002/adma.202312530

[17] N. Di Trani, A. Pimpinelli, and A. Grattoni, "Finite-size charged species diffusion and ph change in nanochannels," *ACS Appl. Mater. Interfaces*, vol. 12, pp. 12246–12255, Feb. 2020. Available: https://doi.org/10.1021/acsami.9b19182

[18] N. Di Trani, N. Racca, D. Demarchi, and A. Grattoni, "Comprehensive analysis of electrostatic gating in nanofluidic systems," *ACS Appl. Mater. Interfaces*, vol. 14, p. 07, no. 31, 2022. Available: https://doi.org/10.1021/acsami.2c08809

[19] N. Di Trani et al., "Electrostatically gated nanofluidic membrane for ultra-low power controlled drug delivery," *Lab Chip*, vol. 20, pp. 1562–1576, 2020.

[20] N. Di Trani et al., "Long-acting tunable release of amlodipine loaded PEG-PCL micelles for tailored treatment of chronic hypertension," *Nanomed. Nanotechnol. Biol. Med.*, vol. 37, Jun. 2021, Art. no. 102417.

[21] N. Di Trani, A. Silvestri, Y. Wang, D. Demarchi, X. Liu, and A. Grattoni, "Silicon nanofluidic membrane for electrostatic control of drugs and analytes elution," *Pharmaceutics*, vol. 12, Jul. 2020, Art. no. 679.

[22] B. Yue, R. Brendel, A. Lukitsch, T. Prentice, and B. Doty, "Solubility and stability of baclofen 3 mg/ml intrathecal formulation and its compatibility with implantable programmable intrathecal infusion systems: Baclofen 3 mg/ml for intrathecal infusion," *Neuromodulation: Technol. Neural Interface*, vol. 20, pp. 397–404, Oct. 2016. Available: https://doi.org/10.1111/ner.12535

[23] F. Del Bono, N. Di Trani, D. Demarchi, A. Grattoni, and P. Motto Ros, "Active implantable drug delivery systems: engineering factors, challenges, opportunities," *Lab Chip*, vol. 25, no. 15, pp. 3608–3629, 2025. Available: https://doi.org/10.1039/d5lc00131e

[24] F. Del Bono, A. Bontempi, N. Di Trani, D. Demarchi, A. Grattoni, and P. M. Ros, "Wireless power transfer closed-loop control for low-power active implantable medical devices," in *Proc. IEEE Sensors*, 2022, pp. 1–4.

[25] F. Del Bono et al., "Design of a closed-loop wireless power transfer system for an implantable drug delivery device," *IEEE Sensors J.*, vol. 24, no. 6, pp. 7345–7354, Mar, 2024.

[26] F. Del Bono, N. Di Trani, D. Demarchi, A. Grattoni, and P. M. Ros, "System integration of an implantable drug delivery device for long-term in-vivo experiments," in *Proc. IEEE Sensors*, 2024, pp. 1–4.

[27] B. Lee, M. Kiani, and M. Ghovanloo, "A smart wirelessly powered homecage for long-term high-throughput behavioral experiments," *IEEE Sensors J.*, vol. 15, no. 9, pp. 4905–4916, Sep. 2015. [Online]. Available: https://ieeexplore.ieee.org/document/7103283.

[28] S. A. Mirbozorgi, H. Bahrami, M. Sawan, and B. Gosselin, "A smart cage with uniform wireless power distribution in 3D for enabling long-term experiments with freely moving animals," *IEEE Trans. Biomed. Circuits Syst.*, vol. 10, no. 2, pp. 424–434, Apr. 2016. [Online]. Available: https://ieeexplore.ieee.org/document/7109946.

[29] E. G. Kilinc, G. Conus, C. Weber, B. Kawkabani, F. Maloberti, and C. Dehollain, "A system for wireless power transfer of micro-systems in-vivo implantable in freely moving animals," *IEEE Sensors J.*, vol. 14, no. 2, pp. 522–531, Feb. 2014. [Online]. Available: https://ieeexplore.ieee.org/document/6623079.

[30] U.-M. Jow, M. Kiani, X. Huo, and M. Ghovanloo, "Towards a smart experimental arena for long-term electrophysiology experiments," *IEEE Trans. Biomed. Circuits Syst.*, vol. 6, no. 5, pp. 414–423, Oct. 2012. [Online]. Available: https://ieeexplore.ieee.org/document/6305491.

[31] E. S. Hawley, E. L. Hargreaves, J. L. Kubie, B. Rivard, and R. U. Muller, "Telemetry system for reliable recording of action potentials from freely moving rats," *Hippocampus*, vol. 12, no. 4, pp. 505–513, 2002. [Online]. Available: https://doi.org/10.1002/hipo.10040.

[32] S. Xu, S. K. Talwar, E. S. Hawley, L. Li, and J. K. Chapin, "A multi-channel telemetry system for brain microstimulation in freely roaming animals," *J. Neurosci. Methods*, vol. 133, nos. 1-2, pp. 57–63, 2004, doi: 10.1016/j.jneumeth.2003.09.012.

[33] T. A. Szuts et al., "A wireless multi-channel neural amplifier for freely moving animals," *Nat. Neurosci.*, vol. 14, no. 2, pp. 263–269, 2011.

[34] N. Di Trani et al., "Remotely controlled nanofluidic implantable platform for tunable drug delivery," *Lab Chip*, vol. 19, no. 13, pp. 2192–2204, 2019. Available: https://doi.org/10.1039/C9LC00394K

[35] N. Di Trani et al., "Extending drug release from implants via transcutaneous refilling with solid therapeutics," *Adv. Therapeutics*, vol. 5, no. 2, 2022, Art. no. 2100214. [Online]. Available: https://pmc.ncbi.nlm.nih.gov/articles/PMC9268610/.

[36] OpenJS Foundation, "Node-red: Flow-based programming for the internet of things," accessed: Jan. 2026. [Online]. Available: https://nodered.org, n.d.

[37] *CC2640R2F SimpleLink™ Bluetooth® 5.1 Low Energy Wireless MCU*, Texas Instruments, Inc., 12 2016, revised 09 2020.

[38] MAX5532–MAX5535 *Dual, Ultra-Low-Power, 12-Bit, Voltage-Output DACs*, Analog Devices, Inc., 03 2020, rev. 2.

[39] TMP117 High-Accuracy, *Low-Power, Digital Temperature Sensor With SMBus™ - and I2C-Compatible Interface*, Texas Instruments, Inc., 06 2018, revised 09 2022.

[40] *TPS82740x 360-nA I_Q MicroSIP™ Step Down Converter Module for Low Power Applications*, Texas Instruments, Inc., 06 2014, revised 06 2014.

[41] E. Ayoub and N. Karami, "Review on the charging techniques of a li-ion battery," in *Proc. 3rd Int. Conf. Technol. Adv. Elect., Electronics Computer Eng. (TAEECE)*, 2015, pp. 50–55.

[42] *LTC4125. 5W AutoResonant Wireless Power Transmitter*, Analog Devices, Inc., 11 2015.

[43] W. Elektronik, "Datasheet: 760308101104 – we-WPCC wireless power charging coil," n.d. Accessed: Apr. 15, 2025. [Online]. Available: https://www.we-online.com/components/products/datasheet/760308101104.pdf

[44] W. Elektronik, "Datasheet: 760308101214 – we-WPCC wireless power charging coil," n.d. accessed: Apr. 15, 2025. [Online]. Available: https://www.we-online.com/components/products/datasheet/760308101214.pdf

[45] "*IEEE Standard for Safety Levels with Respect to Human Exposure to Radio Frequency Electromagnetic Fields*," 3 *kHz to 300 GHz, IEEE International Committee on Electromagnetic Safety Std.* IEEE Std C95.1-2005, 2005.

[46] Texas Instruments, "Simplelink cc2640r2 SDK – simple peripheral example (ble5-stack)," n.d. Accessed: Apr. 15, 2025. [Online]. Available: https://software-dl.ti.com/simplelink/esd/simplelink_cc2640r2_sdk/2.20.00.49/exports/examples/rtos/CC2640R2_LAUNCHXL/ble5stack/simple_peripheral/README.html

[47] Tektronix, Inc., "Keithley dmm7510 7 1/2-digit graphical sampling multimeter," n.d. Accessed: Apr. 15, 2025. [Online]. Available: https://www.tek.com/en/products/keithley/digital-multimeter/dmm7510

[48] *DMM7510 7 1/2-Digit Graphical Sampling Multimeter*, Tektronix, Inc., 02 2018.

[49] G. Jauch Quartz, "Lithium polymer batteries–Jauch quartz," n.d. Accessed: Apr. 15, 2025. [Online]. Available: https://www.jauch.com/en-US/products/battery_technology/getPrm/batteries/Lithium%20Polymer%20Batteries/

[50] M. Moran, R. Roy, C. Wade, B. Corbin, and R. Grindeland, "Size constraints of telemeters in rats," *J. Appl. Physiol.*, vol. 85, no. 4, pp. 1564–71, 1998.

[51] I. Williams, et al., "Senseback – implant considerations for an implantable neural stimulation and recording device," in *Proc. IEEE Biomed. Circuits Syst. Conf. (BioCAS)*, 2019, pp. 1–4.

[52] A. Geipel, F. Goldschmidtboeing, P. Jantscheff, N. Esser, U. Massing, and P. Woias, "Design of an implantable active microport system for patient specific drug release," *Biomed. Microdevices*, vol. 10, no. 4, pp. 469–478, 8 2008.

[53] L. Lewejohann, K. Schwabe, C. Häger, and P. Jirkof, "Impulse for animal welfare outside the experiment," *Laboratory Animals*, vol. 54, no. 2, pp. 150–158, 2020. Available: https://doi.org/10.1177/0023677219891754

[54] Formlabs, "Form 3b – dental and medical 3D printer," n.d. Accessed: Apr. 15, 2025. [Online]. Available: https://formlabs.com/3d-printers/form-3b/
[55] Formlabs, "Biomed durable resin – strong, impact-resistant medical resin," n.d. Accessed: April 15, 2025. [Online]. Available: https://formlabs.com/store/materials/biomed-durable-resin/
[56] Epoxy Technology Inc., "Technical data sheet: Epo-tek® og116," n.d. Accessed: Apr. 15, 2025. [Online]. Available: https://www.epotek.com/docs/en/Datasheet/OG116.pdf
[57] Lomir Biomedical Inc., "Rat jackets – rodent jackets for research applications," n.d. Accessed: Apr. 15, 2025. [Online]. Available: https://www.lomir.com/rodent-jackets/rat-jackets/

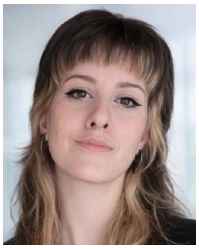

Fabiana Del Bono (Member, IEEE) received the B.Sc. degree in biomedical engineering from the Politecnico di Torino, in 2018, the M.Sc. degree in biomedical engineering from the Politecnico di Torino, Italy, in 2020, and from the Politecnico di Milano, Italy, in 2021, and the Ph.D. degree in electrical, electronics and communications engineering from the Politecnico di Torino, Italy, in 2025. She is currently a Postdoctoral Researcher with the eLiONS - electronic Life-Oriented iNtelligent Systems Group. From 2021 to 2024, she served as a member of the Executive Committee of the IEEE Student Branch of Politecnico di Torino, where she held the role of Webmaster, a Vice-Chair, and a Chair. Her research interests include the design of implantable medical devices, bioelectronics, and wireless power transfer and communication systems for medical applications.

Nicola Di Trani received the B.S. and M.S. degrees in biomedical engineering from the Politecnico of Turin, Turin, Italy, in 2015 and 2017, respectively, and the Ph.D. degree in material science and engineering from the University of Chinese Academy of Sciences. He is currently a Postdoctoral Fellow with the Laboratory of Dr. Alessandro Grattoni, Houston Methodist Research Institute, Houston, Texas, USA. During his Ph.D. and postdoc he has been working on the development of implantable devices for drug delivery. These devices are aimed at the treatment and/or management of a variety of chronic pathologies including hypertension, cancer and HIV prophylaxis. He is the author and co-author of more than 20 peer-reviewed scientific publications in the field of drug delivery, nanofluidics, HIV PrEP, cancer, and material science.

Ashley Joubert graduated from Vet Tech Institute of Houston in 2010 and has been a Licensed Veterinary Technician for over a decade. She is currently working toward the B.Sc. in veterinary technology with the University of Missouri. She formerly a Research Technician with Alessandro Grattoni's Lab, she serves as the IACUC Liaison with Rice University, where she leads efforts in post-approval monitoring. Her work supports balanced science and regulatory compliance that promote both innovation and animal welfare. She is dedicated to fostering a culture of integrity, transparency, and ethical research practices in animal studies.

Camden Caffey received the B.S. degree in chemistry from Texas State University, in 2023. She is currently a Research Assistant with Dr. Alessandro Grattoni's Lab, Houston Methodist Research Institute. Her work involves rodent and non-human primate models, supporting research involving implantable drug delivery systems for HIV PrEP. She plays an integral role in executing in vivo studies and contributing to the lab's translational research efforts.

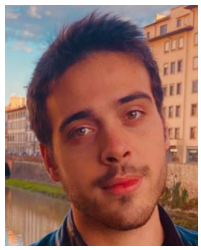

Andrea Dentis (Graduate Student Member, IEEE) received the B.Sc. degree in biomedical engineering and the M.Sc. degree in mechatronics engineering in 2020 and 2023, respectively, from the Politecnico di Torino, Turin, Italy, where he is currently working toward the Ph.D. degree with the Department of Electronics and Telecommunication (DET). His research focuses on the design of inductive wireless power transfer systems for active implantable medical devices.

Danilo Demarchi (Senior Member, IEEE) received the B.E. and Ph.D. degrees in electronics engineering from the Politecnico di Torino, Italy, in 1991 and 1995, respectively. He is a Full Professor with the Politecnico di Torino, Department of Electronics and Telecommunications, Turin, Italy. He is a Visiting Professor with Tel Aviv University (2018–2021) and with EPFL Lausanne (2019). He is a Visiting Scientist with MIT and Harvard Medical School (2018). He is an author and co-author of five patents and more than 300 international scientific publications. He is the Leader of the eLiONS (electronic Life-Oriented iNtelligent Systems) Laboratory, Politecnico di Torino, a member of the IEEE Sensors Council, a member of the IEEE BioCAS Technical Committee, an Associate Editor of IEEE SENSORS JOURNAL, IEEE OPEN JOURNAL OF ENGINEERING IN MEDICINE AND BIOLOGY and Springer *Journal BioNanoScience*, a General Chair of IEEE BioCAS 2017 and a Founder of the IEEE FoodCAS Workshop (Circuits and Systems for Better Quality Food).

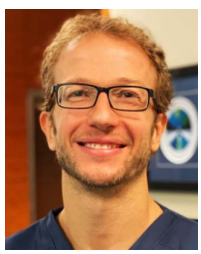

Alessandro Grattoni received the M.S. and Ph.D. degrees in mechanical and biomedical engineering from the Politecnico di Torino, Italy, in 2005 and 2009, respectively. He completed postdoctoral training in nanotechnology with the University of Texas Health Science Center, Houston, in 2010. That same year, he joined the Department of Nanomedicine, Houston Methodist Research Institute (HMRI), where he is currently the Frank J. and Jean Raymond Centennial Chair, a Chairman, and Professor. Dr. Grattoni's research focuses on implantable technologies for long-acting drug delivery and cell transplantation, with applications in HIV PrEP, metabolic syndrome, and cancer immunoradiotherapy. He also investigates electrokinetic nanofluidics for remote drug delivery and 3-D microencapsulation for endocrine cell transplantation in type 1 diabetes and hypogonadism. He established the Center for Space Nanomedicine at HMRI, leveraging the ISS microgravity lab for translational nanomedicine. He is the Founder and a Scientific Advisor to Semper Therapeutics and NanoGland.

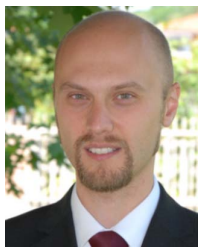

Paolo Motto Ros (Member, IEEE) received the M.Sc. and Ph.D. degrees in electronic engineering from the Politecnico di Torino, Italy, in 2005 and 2009, respectively. He is a Tenure-Track Assistant Professor with the Department of Electronics and Telecommunications, Politecnico di Torino, Turin, Italy. He is a Postdoctoral Researcher with the Politecnico di Torino (2009–2012), a Senior (since 2014) Postdoctoral Researcher with the Istituto Italiano di Tecnologia (2012–2019), a Senior Postdoctoral Researcher and an Adjunct Professor (since 2017) with the Politecnico di Torino (2019–2022); an Assistant Professor with the Politecnico di Torino (2022–2025). He is author and co-author of more than 100 scientific publications in international journals and peer-reviewed conference proceedings. He was a Program Co-Chair of ApplePies 2024 and 2025, member of the Organizing Committee of IEEE ICECS 2019, the FoodCAS Satellite Event at IEEE ISCAS 2021, and IEEE CAFE 2023; Review Committee Member of IEEE BioCAS 2021–2024, Special Session Organizer at IEEE MeMeA 2021, a Program Committee Member of IEEE LASCAS 2022 and 2023, a Guest Editor of MDPI Sensors and a Guest Associate Editor of *Frontiers in Neurorobotics*. He is an Associate Editor of IEEE TRANSACTIONS ON BIOMEDICAL CIRCUITS AND SYSTEMS and IEEE TRANSACTIONS ON AGRIFOOD ELECTRONICS.

Open Access funding provided by 'Politecnico di Torino 2025-2027 Deposit Account' within the CRUI CARE Agreement